Metabolism and Chemical Biology

Cancer Research

# Cancer-Associated Fibroblasts Drive Glycolysis in a Targetable Signaling Loop Implicated in Head and Neck Squamous Cell Carcinoma Progression

Dhruv Kumar[1], Jacob New[1,2], Vikalp Vishwakarma[1], Radhika Joshi[3], Jonathan Enders[2], Fangchen Lin[3], Sumana Dasari[3], Wade R. Gutierrez[1], George Leef[3], Sivapriya Ponnurangam[4], Hemantkumar Chavan[5], Lydia Ganaden[1], Mackenzie M. Thornton[1], Hongying Dai[6], Ossama Tawfik[7], Jeffrey Straub[1], Yelizaveta Shnayder[1], Kiran Kakarala[1], Terance Ted Tsue[1], Douglas A. Girod[1], Bennett Van Houten[8], Shrikant Anant[4,9], Partha Krishnamurthy[5], and Sufi Mary Thomas[1,2,9]

## Abstract

Despite aggressive therapies, head and neck squamous cell carcinoma (HNSCC) is associated with a less than 50% 5-year survival rate. Late-stage HNSCC frequently consists of up to 80% cancer-associated fibroblasts (CAF). We previously reported that CAF-secreted HGF facilitates HNSCC progression; however, very little is known about the role of CAFs in HNSCC metabolism. Here, we demonstrate that CAF-secreted HGF increases extracellular lactate levels in HNSCC via upregulation of glycolysis. CAF-secreted HGF induced basic FGF (bFGF) secretion from HNSCC. CAFs were more efficient than HNSCC in using lactate as a carbon source. HNSCC-secreted bFGF increased mitochondrial oxidative phosphorylation and HGF secretion from CAFs. Combined inhibition of c-Met and FGFR significantly inhibited CAF-induced HNSCC growth *in vitro* and *in vivo* ($P < 0.001$). Our cumulative findings underscore reciprocal signaling between CAF and HNSCC involving bFGF and HGF. This contributes to metabolic symbiosis and a targetable therapeutic axis involving c-Met and FGFR.

**Significance:** HNSCC cancer cells and CAFs have a metabolic relationship where CAFs secrete HGF to induce a glycolytic switch in HNSCC cells and HNSCC cells secrete bFGF to promote lactate consumption by CAFs. *Cancer Res; 78(14); 3769–82. ©2018 AACR.*



## Introduction

Head and neck squamous cell carcinoma (HNSCC) is the fifth most common cancer globally and represents more than 90% of all head and neck cancers. Despite current scientific and therapeutic advancements, there has been no significant improvement in HNSCC patient survival over the past four decades (1). Conventional treatment options, including surgical resection with radiotherapy and/or chemotherapy, are associated with a low 5-year survival. Treatment failure with tumor recurrence is common among patients with HNSCC (2). The poor therapeutic responses underscore the need for an improved understanding of the tumor biology.

Over the past few decades, there has been a growing interest in the tumor microenvironment and its role in tumor progression and response to therapy. In addition to cancer cells, a tumor comprises many stromal components, which include tumor-infiltrating immune cells, endothelial cells, neuronal cells, lymphatic cells, cancer-associated fibroblasts (CAF), and the extracellular matrix (3). In HNSCC, the surrounding stroma contains an abundance of CAFs. Previous studies have reported that CAFs secrete HGF (4, 5). Furthermore, CAF-secreted HGF binds and activates c-Met tyrosine kinase receptor on HNSCC cells triggering proliferation, invasion, and migration (5). HNSCC likely modulates the microenvironment CAFs by secreting basic FGF (bFGF). Several cancer types secreted bFGF, including HNSCC (6). Secreted bFGF binds to FGFR expressed on the cell surface of several cell types and regulates proliferation and migration (7). FGFR inhibition reduces HNSCC growth stimulated by human foreskin fibroblasts (8). Although the autocrine regulation of bFGF is documented, little is known about the paracrine regulation of bFGF between HNSCC and CAFs. Furthermore, the role of CAFs in HNSCC metabolism has not been elucidated.

[1]Department of Otolaryngology, University of Kansas Medical Center, Kansas City, Kansas. [2]Department of Anatomy and Cell Biology, University of Kansas Medical Center, Kansas City, Kansas. [3]Department of Otolaryngology, University of Pittsburgh School of Medicine, Pittsburgh, Pennsylvania. [4]Department of Surgery, University of Kansas Medical Center, Kansas City, Kansas. [5]Department of Pharmacology, Toxicology & Therapeutics, University of Kansas Medical Center, Kansas City, Kansas. [6]Health Services & Outcomes Research, Children's Mercy Hospital, Kansas City, Missouri. [7]Department of Pathology, University of Kansas Medical Center, Kansas City, Kansas. [8]Department of Pharmacology and Chemical Biology, University of Pittsburgh School of Medicine, Pittsburgh, Pennsylvania. [9]Department of Cancer Biology, University of Kansas Medical Center, Kansas City, Kansas.

**Note:** Supplementary data for this article are available at Cancer Research Online (http://cancerres.aacrjournals.org/).

D. Kumar, J. New, and V. Vishwakarma contributed equally to this article.

Current address for D. Kumar: Amity Institute of Molecular Medicine & Stem Cell Research, Amity University, Noida 201313, Uttar Pradesh, India.

**Corresponding Author:** Sufi Mary Thomas, University of Kansas Medical Center, 3901 Rainbow Blvd., Wahl Hall East 4031, Mailstop 3040, Kansas City, KS 66160. Phone: 913-588-6664; Fax: 913-588-4676; E-mail: sthomas7@kumc.edu

**doi:** 10.1158/0008-5472.CAN-17-1076

Unlike normal cells, malignant cells often display increased glycolysis, even in the presence of oxygen, a phenomenon known as the Warburg effect. The metabolic reprogramming of cancer cells leads to the extensive use of glucose for their growth and survival (9). Cells use two major pathways to produce ATP: glycolysis and mitochondrial respiration through oxidative phosphorylation (OXPHOS). The glycolytic pathway involves a series of reactions that converts glucose to pyruvate, resulting in ATP, NADH, and hydrogen ions. Pyruvate can have three fates: conversion to lactate, conversion of acetyl-CoA, or conversion to alanine (10). In the conversion of pyruvate to lactate, NADH and hydrogen ions are consumed by LDH5. Lactate and hydrogen ions are pumped out of the cell by several mechanisms to maintain homeostasis of the intracellular pH. The release of protons out of the cell results in extracellular acidification. Pyruvate is also converted to acetyl-CoA by pyruvate dehydrogenase to enter the mitochondria and undergo OXPHOS. In many nontransformed differentiated cells, such as neurons and fibroblasts, OXPHOS produces most of the cellular ATP. In contrast, cancer cells heavily depend on glycolysis for ATP production. This is supported by the fact that HNSCC has increased lactate levels, which correlates with reduced survival (11). The mechanisms whereby HNSCC tumors survive highly acidic conditions remain unknown; yet, elucidation would provide potential therapeutic targets. In addition, comprehensive studies elucidating cross-talk between HNSCC and the surrounding CAFs are lacking. We hypothesized that CAF-secreted HGF regulates HNSCC metabolism and HNSCC-secreted bFGF and lactate regulate CAF proliferation and mitochondrial OXPHOS. Our data elucidate a dynamic reciprocal signaling between HNSCC and CAFs. Finally, building on this mechanistic insight, we demonstrate the efficacy of simultaneous inhibition of c-Met and FGFR as a therapeutic approach for HNSCC.

## Materials and Methods

### Cell culture

Patient samples were collected under the auspices of the Biospecimen Repository Core at the University of Kansas Cancer Center (Kansas City, KS) with written informed consent from patients, using protocols approved by the Human Subjects Committee at the University of Kansas Medical Center, in accordance with the U.S. Common Rule (45 CFR 46). CAFs were isolated from HNSCC patient samples by dissecting the sample into <2-mm components, and allowing the sample to adhere to 10-cm culture dish. CAFs are characterized by their expression of α-smooth muscle actin, and lack of expression of cytokeratin-14, as we demonstrate in our previous publication (5). CAFs were cultured for less than 12 passages to ensure biologic similarity to the original specimen. Well-characterized HNSCC cell lines UM-SCC-1, HN5, and OSC-19 (gifts from Dr. Thomas E. Carey, University of Michigan, Ann Arbor, MI; Dr. Jeffrey N. Myers, MD Anderson Cancer Center, Houston, TX; and Dr. Jennifer R. Grandis, University of Pittsburgh, Pittsburgh, PA, respectively, obtained in 2013–2014) all authenticated in 2017 by STR profiling (University of Arizona Genetics Core, Tucson, AZ), and confirmed to be negative of *Mycoplasma* using PCR Mycoplasma Test Kit (MD Biosciences), were used in this study (12). HNSCC cells and primary CAF lines were cultured and maintained in DMEM supplemented with 10% FBS in a humidified 37°C incubator with 5% $CO_2$. In all experiments, results obtained from primary patient lines were confirmed using at least two different patient samples. Conditioned media were collected from a 95% confluent flask of either cancer cells or fibroblasts for a period of 24 hours for cancer cells and 72 hours for fibroblasts with serum-free DMEM.

### Reagents

Growth factors, bFGF (#F0291) and HGF (#H5791), were obtained through Sigma Aldrich. PF-02341066 (crizotinib) was obtained from Active Biochem and AZD-4547 was obtained from Chemietek.

Primary antibodies used are as follows: HKII (#2867), phospho-p44/42 MAPK (#4370), bFGF (#3196), and TFAM (#8076) were obtained from Cell Signaling Technology; MCT1 (NBP1-59656) was obtained from Novus Biologicals; FGFR1 (E10580), FGFR2 (E10570), and FGFR3 (E10230) were obtained from Spring Bioscience; FGFR4 was obtained from R&D Systems. β-Tubulin (T0198) was obtained from Sigma Aldrich. β-Actin (#sc-1616) was obtained from Santa Cruz Biotechnology. Secondary anti-rabbit IgG Dylight 680 (#35568), anti-rabbit IgG Dylight 488 (#35553), and anti-mouse IgG Dylight 800 (#35521) were from Thermo Fisher Scientific.

Primer sequences used are as follows: bFGF (F: CTGTACTGCAAAAACGGG; R: AAAGTATAGCTTTCTGCC), c-MET (F: CATGCCGACAAGTGCAGTA; R: TCTTGCCATCATTGTCCAAC), HGF (F: ATCAGACACCACACCGGCACAAAT; R: GAAATAGGGCAATAATCCCAAGGAA), HKII (F: CAAAGTGACAGTGGGTGTGG; R: GCCAGGTCCTTCACTGTCTC), PFK-1 (F: GGCTACTGTGGCTACCTGGC; R: GCATGGAGTACAGGGAAACC), PGC-1α (F: CCGCACGCACCGAAATTCTC; R: GCCTTCTGCCTGTGCCTCTC), TIGAR (F: CGGAATTCAGAACAGTTTTCCCAAGGATCTCC; R: CGGAATTCAACCTTAGCGAGTTTCAGTCAGTCC), and β-actin (F: AGGGGCCGGACTCGTCATACT; R: GGCGGCACCACCATGTACCCT) were all obtained from Thermo Fisher Scientific.

### Measurement of glycolysis and OXPHOS in HNSCC and CAFs

Extracellular acidification and oxygen consumption rates (ECAR and OCR, respectively) were measured using the XF24 extracellular flux analyzer (Seahorse Bioscience). To assess the effects of conditioned media or growth factors, cells were cultured in serum-free media for 24 hours and then exposed to conditioned media or growth factor, with or without inhibitors as applicable, for 48 hours. Cells were washed with unbuffered DMEM and equilibrated with 700 μL of prewarmed unbuffered DMEM containing 1 mmol/L sodium pyruvate at 37°C for 30 minutes. Seahorse reagent concentrations are as follows: oligomycin, 1 μmol/L (Sigma, O4876); 2-deoxyglucose, 100 mmol/L (Sigma, D6134); glucose, 910 μmol/L (Sigma, G5400); rotenone, 1 μmol/L (Sigma, R8875); FCCP, 0.3 μmol/L (Sigma, C2920); all flux analyses were normalized to protein content (assessed by Bradford assay) within individual wells.

### Immunoblotting

Whole-cell lysates were prepared using RIPA lysis buffer with a mixture of protease and phosphatase inhibitors (Minitab, Thermo Fisher Scientific) on ice. Equal amount of proteins were separated through a 10% SDS-PAGE. Blots were blocked with Odyssey blocking buffer, incubated with primary antibody overnight at 4°C, and dylight-conjugated secondary antibody for 1 to 2 hours. Protein bands were detected using the LI-COR odyssey protein imaging system. Immunoblots for data presented were

analyzed from at least three experimental repeats. Densitometric analyses were performed with ImageJ (v1.50i).

### Immunofluorescence

HNSCC and CAFs were plated in 8-well chamber slides ($1 \times 10^4$ cells/well; in combination group, $5 \times 10^3$ cells of each cell type were plated to maintain consistent cell number) under serum-free conditions for 48 hours. Methanol (70%) was used to fix cells, and subsequently, cells were treated with permeabilization buffer [Triton X-100 (0.5%) in PBS]. Two percent BSA in PBS solution was used to block cells. Cells were incubated in primary antibody overnight (1:100 concentration at 4°C). Dylight-conjugated antibody was used to detect primary antibodies. Slides were mounted with a coverslip in VECTASHIELD mounting media, and images were captured on Nikon Eclipse TE2000 inverted microscope with a photometrics coolsnap HQ2 camera. Fluorescence intensity was quantified using Metamorph software v. 7.8.0.0.

### RNA analysis

RNA was extracted from harvested cells using TRIzol reagent (Thermo Fisher Scientific) following the manufacturer's instructions. RNA was subjected to DNase digestion prior to cDNA preparation using the SuperScript First-Strand Synthesis System (Invitrogen). PCR products were resolved on agarose gel and imaged. Agarose gel images of RT-PCR data presented were analyzed from at least three experimental repeats. Densitometric analyses were performed with ImageJ (v1.50i).

### Proliferation and migration assays

To assess CAF proliferation, $2 \times 10^3$ cells were plated in a 96-well plate in 10% FBS containing DMEM. The media were then replaced with serum-free DMEM, HNSCC conditioned media, or recombinant bFGF, with or without inhibitors (AZD-4547 or rotenone) for 72 hours. Nuclear content across treatment groups was assessed using the CyQUANT Assay Kit (Thermo Fisher Scientific) per the manufacturer's instructions. Fold change in CAF proliferation relative to the vehicle control was determined.

To determine whether dual inhibition of c-Met and FGFR mitigates CAF-induced HNSCC proliferation in admixed cultures ($2 \times 10^4$ cells of each cell type per 6-well plate), UM-SCC-1 cells were stained with carboxyfluorescein diacetate succinimidyl ester (CFSE) (Thermo Fisher Scientific) per the manufacturer instructions and extensively washed to remove unbound dye. Cells were treated in duplicate with vehicle control (DMSO), AZD-4547 (2 μmol/L), PF-02341066 (1 μmol/L), or a combination of both inhibitors in serum-free DMEM. After 72 hours, cells were trypsinized, washed, fixed in 70% ethanol, and suspended in 100 μL of PBS. CFSE-stained UM-SCC-1 cells were analyzed by flow cytometry at 488 nm. Data are presented as fold change in cell number relative to the vehicle control.

To assess the effect of UM-SCC-1 on CAF migration, CAF cells were seeded in duplicate transwell inserts ($2 \times 10^4$ cells/insert) with a pore size of 8 μm (Thermo Fisher Scientific) in serum-free media. The inserts were placed in the holding-well containing vehicle control (DMSO), UM-SCC-1-CM with or without AZD-4547 (2 μmol/L) for 24 hours. The number of cells that migrated through the transwell chamber was counted in 4 fields after hematoxylin and eosin (H&E) staining using the Hema 3 Kit (Thermo Fisher Scientific) by a blinded observer. Cells were plated in parallel along with the corresponding treatment in 96-well plates to assess cell viability using the CyQUANT Kit (Thermo Fisher Scientific). The number of cells that migrated through the insert was normalized to the cell viability. Fold change in CAF migration in treatment arms relative to the vehicle control was determined.

For single carbon source assessment, Biolog phenotype microarray (Biolog) was used following the manufacturer's instructions. A question was raised for glutamine and palmitate alone, and these were not included on the Biolog plate. To assess these, we plated cells ($1 \times 10^4$ cells/well) in Hank's Balanced Salt Solution (HBSS) with either glucose (Thermo Fisher Scientific) alone, glutamine (Sigma-Aldrich) alone, or palmitate (Sigma-Aldrich) conjugated to BSA (Thermo Fisher Scientific) to dissolve palmitate (BSA as a control was also applied in glucose and glutamine groups) and assessed proliferation over the same time period (72 hours). Results were normalized to glucose.

### siRNA

Cells were transfected with either pooled c-Met siRNA (100 nmol/L; #sc-29397, pooled of three transcripts, Santa Cruz Biotechnology, Inc.) or control siRNA (100 nmol/L; Santa Cruz proprietary control sequence based upon ref. 13; Santa Cruz Biotechnology, Inc.) using Lipofectamine-2000 (Invitrogen) for 4 hours.

### Lactate assessment

Lactate concentration in conditioned media assessed was using L-lactate Assay Kit (Eton Bioscience), per the manufacturer's instructions. Cells were plated ($3 \times 10^5$ cells/dish in a 60-mm dish) in various conditions for 48 hours following 24-hour serum starvation.

### ELISA

Human HGF (#RAB0212) and bFGF (#RAB0182) ELISA Kits were obtained from Sigma-Aldrich. Cytokine levels were assessed in duplicate wells, per the manufacturer's instructions. Cells were plated ($3 \times 10^5$ cells/dish in a 60-mm dish) in various conditions for 48 hours following 24-hour serum starvation.

### *In vivo* studies

All *in vivo* protocols were approved by the KUMC Institutional Animal Care and Use Committee. To assess the *in vivo* efficacy of targeting c-Met and FGFR, 100 μL of admixed HNSCC (UM-SCC-1, $1 \times 10^6$ cells) and CAFs ($0.5 \times 10^6$ cells) in serum-free DMEM were inoculated into the right flank of athymic nude-Foxn1nu mice. Mice were treated with vehicle control (saline with 1% Tween-80), AZD-4547 (15 mg/kg/day), PF-02341066 (15 mg/kg/day), or a combination of AZD-4547 and PF-02341066 via oral gavage, every day 5 days/week for 2 weeks. Tumor diameters were measured in two perpendicular dimensions using a Vernier caliper, and the volume was calculated as described previously (14), briefly (tumor volume = long dimension $\times$ short dimension$^2$ $\times$ 0.52).

### Statistical analysis

Data are reported as the mean ± SEM. For *in vitro* experiments, data were analyzed using Mann–Whitney test for comparison between two groups and Kruskal–Wallis test for comparison of multiple groups. For *in vivo* study, one-way ANOVA test was employed to assess the level of significance in tumor volumes

between treatment arms. Statistical analyses were performed using GraphPad Prism 6 Version 6.03. Statistical significance was claimed at 95% confidence level ($P < 0.05$).

## Results

### HNSCC demonstrates higher glycolytic potential than CAFs

Previously, we reported CAF-conditioned media (CM) regulate HNSCC proliferation, migration, and invasion (5). HNSCC tumors are highly glycolytic and increased glycolysis is associated with tumor progression and metastasis. To elucidate the metabolic preferences of HNSCC and CAFs, we assessed the ECAR and the OCR to determine glycolytic capacity (Fig. 1A) and mitochondrial OXPHOS (Fig. 1B). Compared with CAFs, HNSCC cells demonstrated a significantly higher glycolytic capacity than CAFs ($P < 0.0001$). In contrast, the maximal respiration of CAFs was significantly higher than HNSCC ($P < 0.0001$). To further characterize preferential carbon sources for energy by HNSCC and CAFs, we tested cell proliferation in the presence of a single carbon source. CAFs demonstrate significantly greater growth ($P = 0.0022$) in the presence of lactate as a sole carbon source compared with HNSCC (Fig. 1C). An additional finding was that HNSCCs utilize fructose more efficiently than CAFs, which may be a consequence of the increased glycolysis in HNSCC; however, this finding was not followed in this study. As palmitate and glutamine alone were not included in the Biolog assay plate, we also tested the growth of HNSCC and CAFs exposed to these carbon sources in HBSS and observed no significant differences between HNSCC and CAFs in growth rates to palmitate or glutamine alone (Supplementary Fig. S1A). This single carbon source assay suggests CAFs use lactate more efficiently than HNSCC cells.

### CAF-secreted HGF regulates HNSCC glycolysis through c-Met

We previously reported that paracrine activation c-Met by CAF-secreted HGF is a contributing event to HNSCC progression (4, 5). In addition, c-Met has been linked to glycolysis as c-Met inhibition reduces intracellular NADPH in nasopharyngeal carcinoma cell lines by downregulating TP53-induced glycolysis and apoptosis regulator (TIGAR; ref. 15). NADPH is generated when glucose 6-phosphate is oxidized to ribose 5-phosphate in the pentose phosphate pathway, and through the malic enzyme conversion of malate to pyruvate (16). Importantly, NADPH production correlates with glucose uptake (17). These studies led us to question the role of CAF-secreted HGF in regulating HNSCC glycolysis. Of note, HGF is secreted in the microenvironment by CAFs, not HNSCC, and is readily detectable in CAF-CM (Supplementary Fig. S1B; ref. 4). We found CAF-CM to significantly increase the glycolytic capacity of HNSCC [HN5 ($P = 0.0003$) and UM-SCC-1 ($P = 0.0006$); Fig. 1D and E].

In order to further elucidate the role of HGF in inducing HNSCC glycolysis, HNSCC cells were stimulated with recombinant HGF, with or without c-Met inhibition using PF-02341066 (1 μmol/L). HGF-induced HNSCC glycolysis was inhibited in the presence of PF-02341066 (Fig. 1F and G). Inhibition of HGF-induced ECAR and glycolytic capacity by PF-02341066 demonstrates that glycolysis in HNSCC is regulated by c-Met. To confirm the increased ECAR was a result of glycolysis and not by some other biological pathway, we directly assessed lactate after HGF stimulation of HNSCC cells. We observed HGF to enhance lactate production (Supplementary Fig. S1C). In order to rule out off-target effects of PF-02341066, HNSCC cells were transfected with c-Met siRNA. c-Met knockdown significantly reduced the ability of HGF ($P = 0.0004$) and CAF-CM ($P < 0.0001$) to increase the glycolytic capacity of HNSCC cells (Fig. 1H and I). Met is activated through both ligand, HGF, and ligand-independent means, such as with IGF1 or EGFRvIII (18, 19). PF-02341066 inhibition of c-Met even without HGF applied demonstrates a pronounced decrease in glycolytic capacity (Fig. 1F and G). C-MET silencing with siRNA also demonstrates a decrease in glycolytic capacity (Fig. 1H and I), alongside a decrease in HKII and PFK-1, regardless of HGF stimulation (Supplementary Fig. S1D). As HGF is not secreted by HNSCC, these data support a role for ligand-independent activation of Met in HNSCC glycolysis. Addition of HGF as a ligand further promotes glycolysis.

### c-Met regulates HNSCC glycolysis through hexokinase-II

Hexokinase-II and phosphofructokinase are key rate-limiting enzymes in the glycolytic cascade. Hexokinase-II is highly upregulated in the early stage of tumorigenesis in several cancers including HNSCC (20). Hexokinase-II levels in HNSCC were induced by CAF-CM (Fig. 2A and B; Supplementary Fig. S2A). Furthermore, c-Met inhibition by PF-02341066 mitigated CAF-CM–induced hexokinase-II levels ($P = 0.0364$; Fig. 2A and B). Knockdown of c-Met with siRNA mitigated CAF-CM or HGF-induced hexokinase-II and phosphofructokinase mRNA levels in HNSCC. These results suggest CAF-secreted HGF induces key enzymes in the glycolytic pathway of HNSCC.

Excessive glycolysis is associated with overexpression of the lactate transporter MCT1, which is the best characterized transporter of the MCT family (21). MCT1 is overexpressed in HNSCC (11). We hypothesized CAFs enhance MCT1 levels in HNSCC, facilitating lactate secretion from HNSCC. We observed a significant increase in MCT1 levels in cocultured HNSCC and CAFs as assessed by total fluorescent intensity of the coculture [HN5 ($P = 0.0010$) and UM-SCC-1 ($P = 0.0008$); Fig. 2C–F]. In addition, CAF-CM increased MCT1 protein levels in HNSCC (Supplementary Fig. S2A). To evaluate the role of c-Met in regulating MCT1 levels, we stimulated HNSCC with HGF and with c-Met inhibitor PF-02341066. Treatment with PF-02341066 mitigated HGF-mediated induction of MCT1 levels in HNSCC (Fig. 2G and H). Furthermore, PF-02341066 treatment decreased HGF-induced lactate secretion from HNSCC [HN5 ($P = 0.0087$) and UM-SCC-1 ($P = 0.0125$); Fig. 2I and J]. In addition, CAF-CM increased HNSCC lactate secretion, and knockdown of MCT1 mitigated this secretion (Supplementary Fig. S2B). These data demonstrate that CAFs regulate HNSCC glycolysis by HGF induction of key glycolytic enzymes and lactate efflux through MCT1.

### CAF-secreted HGF regulates bFGF secretion from HNSCC

FGFRs are expressed in myofibroblasts from both normal oral mucosa and HNSCC (22). However, aberrant FGFR signaling plays an important role in the tumor progression (23). A previous report demonstrated bFGF is essential for autocrine and paracrine activation of FGFR (24). We demonstrate the expression of bFGF in HNSCC cell lines and secretion of bFGF in HNSCC-CM (Supplementary Fig. S3A and S3B); furthermore, we observe strong expression of FGFR throughout patient-derived CAFs (Supplementary Fig. S3C).

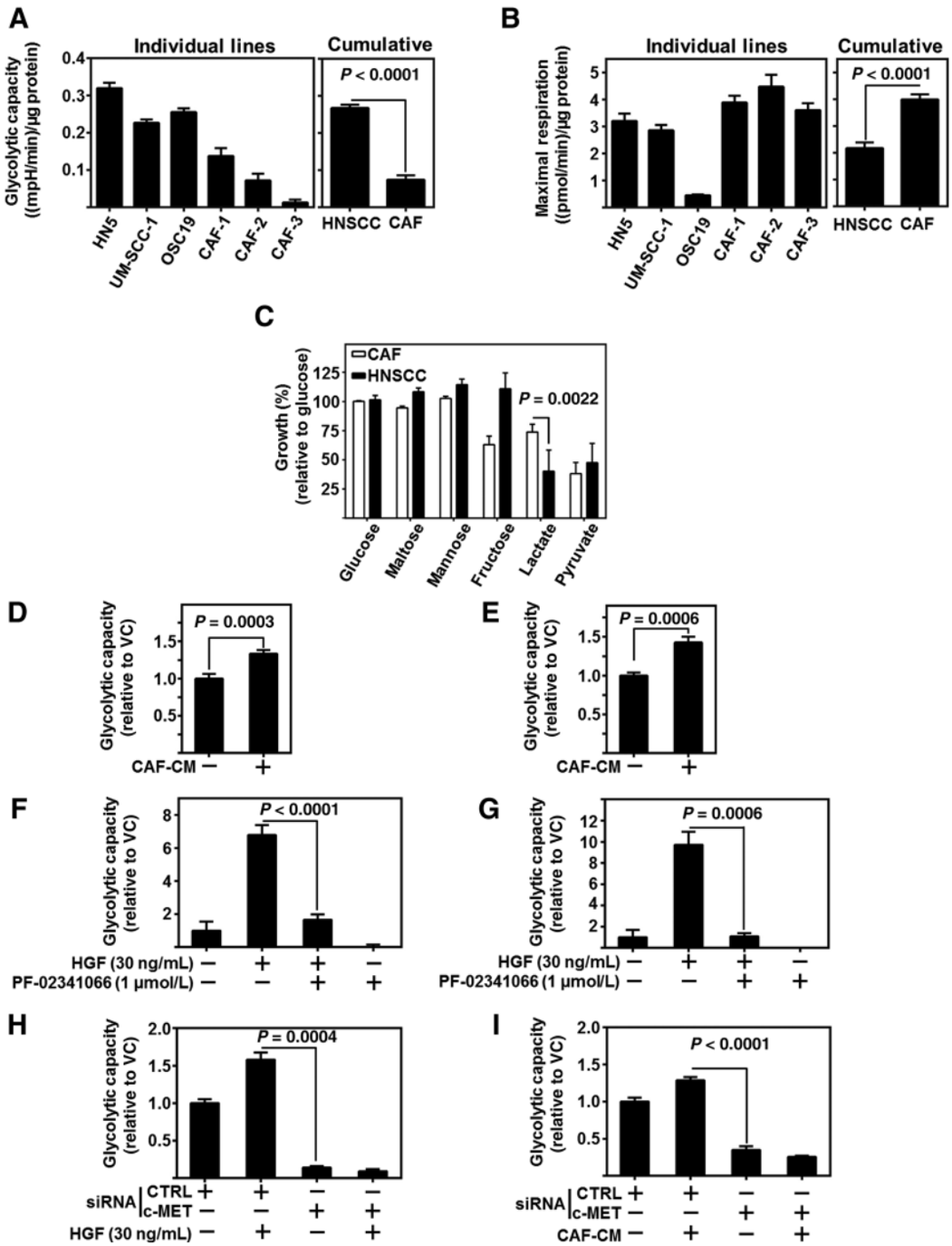


**Figure 1.**

CAFs regulate HNSCC glycolysis through c-Met. **A,** Glycolytic capacity of HNSCC (HN5, UM-SCC-1, OSC19) and three patient-derived CAF lines assessed by Seahorse flux analyzer. Graph represents cumulative results from three independent experiments. Combined graph represents mean of all three HNSCC lines and all three CAF lines. **B,** Maximal respiration of HNSCC (HN5, UM-SCC-1, OSC19) and three patient-derived CAF lines assessed by Seahorse flux analyzer. Graph represents cumulative results from three independent experiments. Combined graph represents mean of all three HNSCC lines and all three CAF lines. **C,** Differential growth of CAFs versus HNSCC in single carbon sources over 72 hours. Data represent cumulative results from four CAF lines and three HNSCC cell lines. **D,** Cumulative results of glycolytic capacity of HN5 exposed to two CAF-CMs. **E,** Cumulative results of glycolytic capacity of UM-SCC-1 exposed to two CAF-CMs. All error bars, ± SEM. **F,** HN5 treated with recombinant HGF (30 ng/mL) and/or c-MET inhibitor, PF-02341066 (1 µmol/L). ECAR normalized to protein content per well. Cumulative results of glycolytic capacity graphed across treatment arms. **G,** UM-SCC-1 treated with recombinant HGF (30 ng/mL) and/or c-MET inhibitor, PF-02341066 (1 µmol/L). ECAR normalized to protein content per well. Cumulative results of glycolytic capacity graphed across treatment arms. **H,** UM-SCC-1 treated with recombinant HGF (30 ng/mL) and either control siRNA (CTRL) or c-MET siRNA. ECAR normalized to protein content per well. Cumulative results of glycolytic capacity graphed across treatment arms. **I,** UM-SCC-1 treated with CAF-CM and either control siRNA (CTRL) or c-MET siRNA. ECAR normalized to protein content per well. Cumulative results of glycolytic capacity graphed across treatment arms.

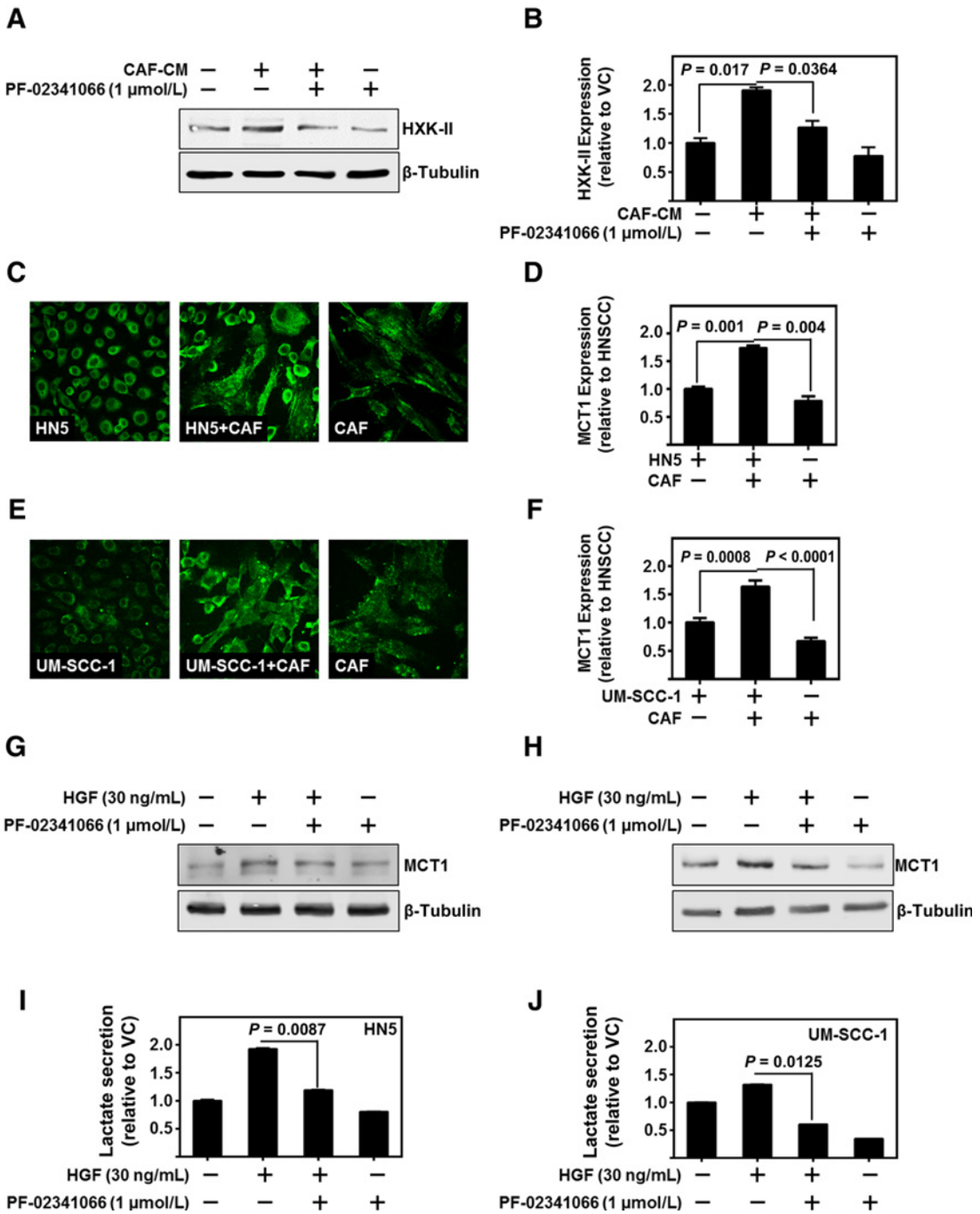


**Figure 2.**

CAF-secreted HGF regulates HNSCC glycolytic enzymes and lactate production. **A** and **B,** Representative immunoblot of hexokinase-II (HXK-II) protein levels of HN5 treated with CAF-CM and/or c-MET inhibitor, PF-02341066 (1 μmol/L). β-Tubulin served as loading control. Cumulative densitometric analysis of hexokinase-II/β-tubulin normalized to vehicle control-treated lane. **C** and **D,** Representative immunofluorescent image (magnification, ×200) of MCT1 (green) on HN5, CAFs, or coculture of HN5 and CAFs. Number of cells kept constant between wells. MCT1 levels were assessed as total fluorescent intensity and cumulative results. **E** and **F,** Representative immunofluorescent image (magnification, ×200) of MCT1 (green) on UM-SCC-1, CAFs, or coculture. Number of cells kept constant between wells. MCT1 levels were assessed as total fluorescent intensity and cumulative results. **G,** Representative immunoblot of MCT1 protein levels expressed in HN5 with treatment of recombinant HGF (30 ng/mL) and/or PF-02341066 (1 μmol/L). β-Tubulin served as loading control. **H,** Representative immunoblot of MCT1 protein levels expressed in UM-SCC-1 with treatment of recombinant HGF (30 ng/mL) and/or PF-02341066 (1 μmol/L). β-Tubulin served as loading control. **I,** Lactate secretion as assessed by enzymatic based absorbance assay of HN5 treated with HGF (30 ng/mL) and/or PF-02341066 (1 μmol/L). Data represent cumulative normalized to vehicle control-treated cells. **J,** Lactate secretion as assessed by enzymatic based absorbance assay of HN5 treated with HGF (30 ng/mL) and/or PF-02341066 (1 μmol/L). Data represent cumulative results normalized to vehicle control-treated cells. Error bars, ± SEM.

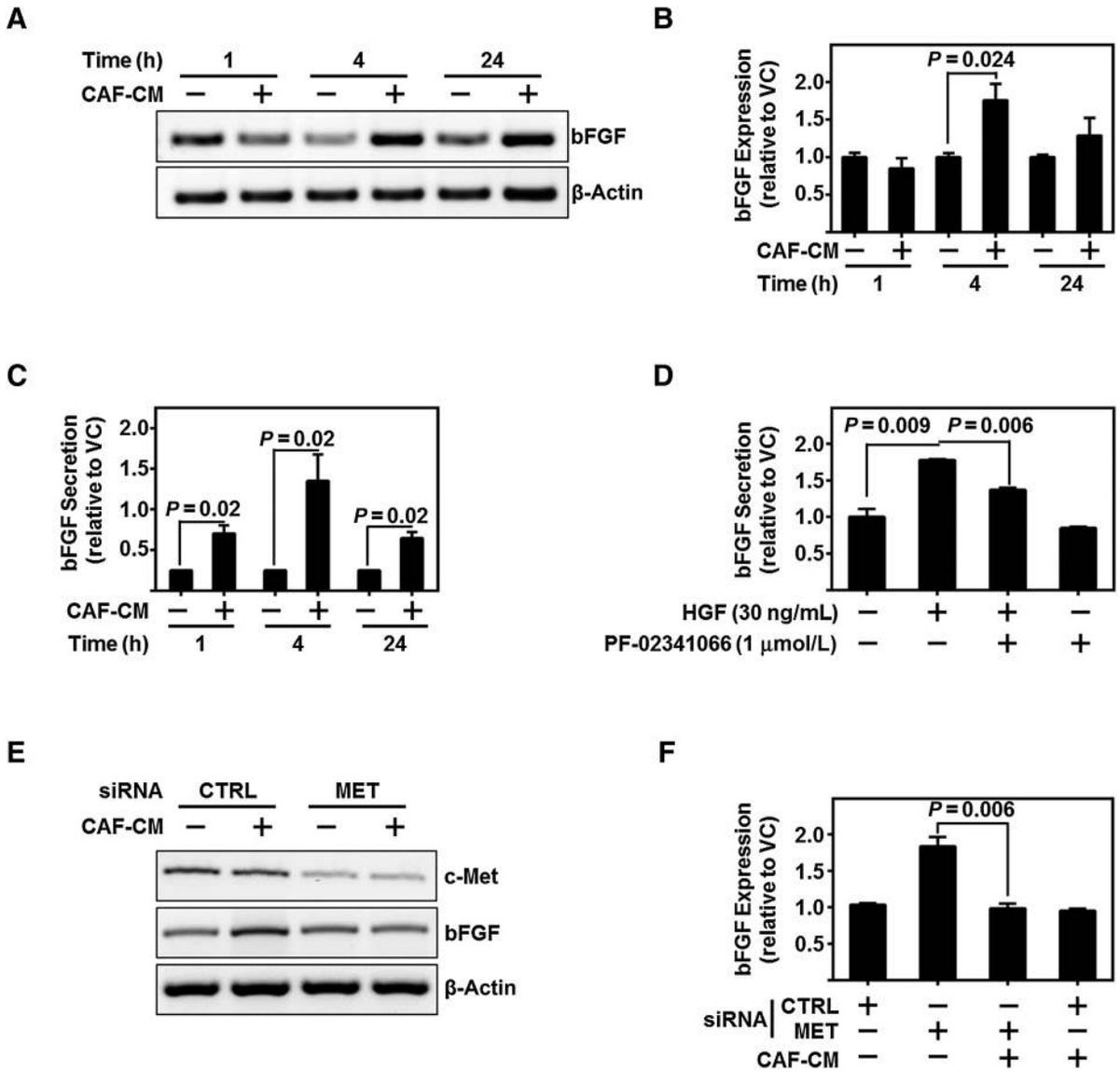


**Figure 3.**

c-Met regulates bFGF expression in HNSCC. **A** and **B,** Representative PCR product of bFGF mRNA in UM-SCC-1 treated with CAF-CM for the indicated time points. β-Actin served as loading control. Graph depicts cumulative densitometric results of three independent experiments of bFGF/β-actin normalized to vehicle control-treated cells at each time point. **C,** Graph depicts ELISA protein assessment of bFGF secreted from HN5 exposed to three different CAF-CMs. Cumulative data from three independent experiments are normalized to vehicle-treated cells at each time point. **D,** Graph depicts ELISA protein assessment of bFGF secreted from UM-SCC-1 exposed to either HGF (30 ng/mL) and/or c-MET inhibitor, PF-02341066 (1 μmol/L). Cumulative data from three independent experiments are normalized to vehicle-treated cells. **E** and **F,** Representative PCR product of c-MET, bFGF, or β-actin (as loading control) mRNA in UM-SCC-1 exposed to CAF-CM with either control siRNA (CTRL) or c-Met siRNA. Cumulative results from three independent experiments of bFGF/β-actin normalized to CTRL siRNA, vehicle-treated UM-SCC-1. Error bars, ± SEM.

We questioned the interplay of CAF-secreted HGF in stimulating bFGF from HNSCC. CAF-CM induced bFGF mRNA expression and protein secretion (Fig. 3A–C). Inhibition of c-Met by either PF-02341066 or siRNA significantly reduced HGF-induced or CAF-CM–induced bFGF secretion from HNSCC ($P = 0.006$; Fig. 3D–F; Supplementary Fig. S3D). Taken together, these data demonstrate CAF-secreted HGF regulates bFGF expression and secretion in HNSCC through c-Met.

### HNSCC-secreted bFGF stimulates OXPHOS, proliferation, and migration in CAFs

Under physiologic conditions, normal cells use OXPHOS to produce cellular energy. In contrast, cancer cells rely heavily on glycolysis to produce energy and promote tumor progression. Recent studies demonstrate metabolic reprograming in CAFs promotes tumor progression (25). For example, highly glycolytic lung tumors reprogram their stromal cells to survive even in low

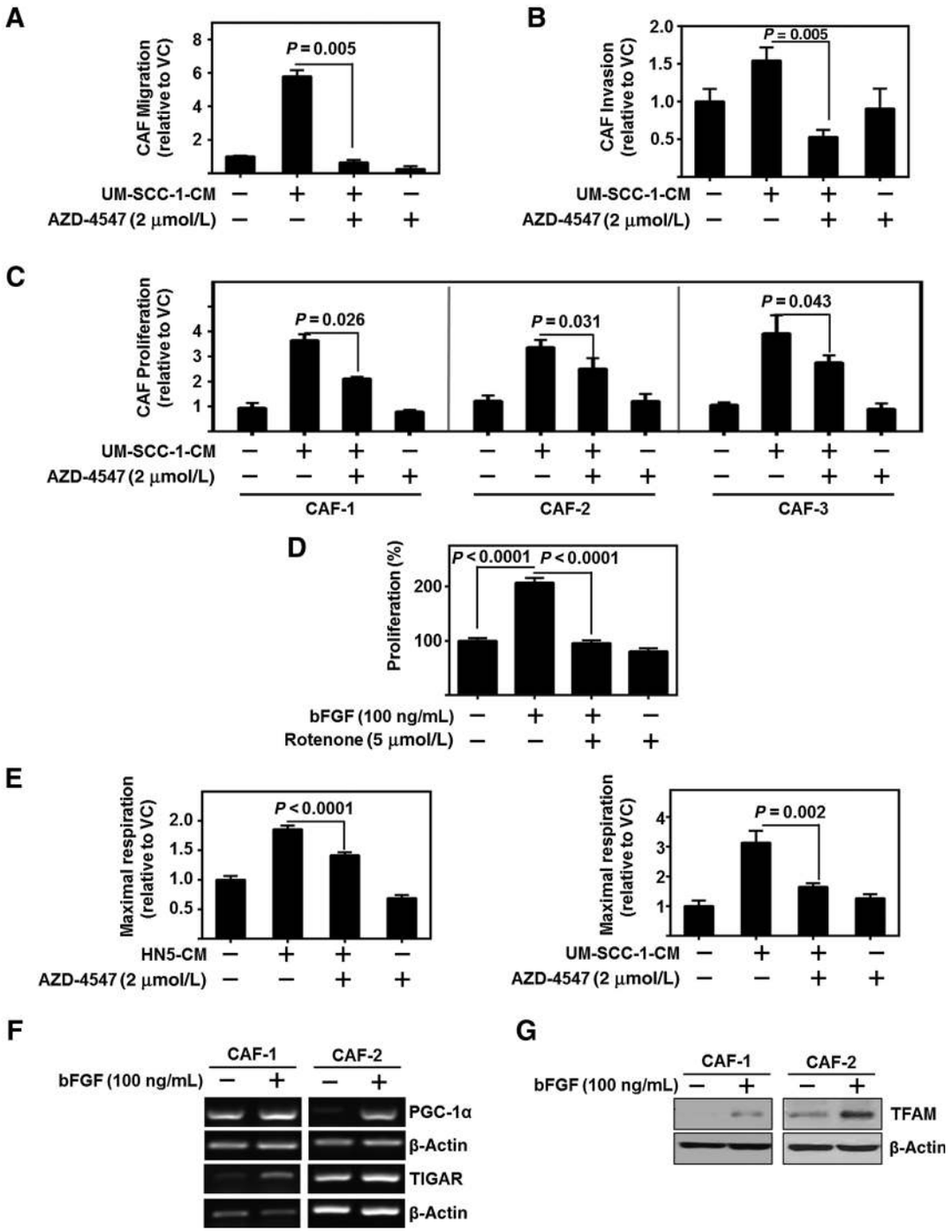


**Figure 4.**

HNSCC regulates CAFs through bFGF induction of OXPHOS. **A,** HNSCC-CM (UM-SCC-1)–enhanced CAF migration is attenuated by AZD-4547 (2 μmol/L). Migration assessed using transwell assay. Data represent cumulative results from three independent experiments and are normalized to cell viability. **B,** HNSCC-CM (UM-SCC-1)–enhanced CAF invasion is attenuated by AZD-4547 (2 μmol/L). Invasion assessed using transwell assay. Data represent cumulative results from three independent experiments and are normalized to cell viability. Error bars, ± SEM. **C,** HNSCC-CM–enhanced CAF proliferation is attenuated by AZD-4547 (2 μmol/L). Three CAF lines were treated with UM-SCC-1-CM and/or AZD-4547. Graphs depict three independent experiments for each cell line. **D,** HNSCC-induced CAF proliferation is dependent on OXPHOS. Proliferation of CAFs in the presence of bFGF (100 ng/mL) and/or rotenone (5 μmol/L). Graph depicts cumulative results of three experiments plated in triplicate; error bars, ± SEM. **E,** CAFs were treated with HN5-CM or UM-SCC-1-CM and/or FGFR inhibitor, AZD-4547 (2 μmol/L). Data normalized to protein content per well. Graph depicts fold change in maximum respiration normalized to basal media control cells. **F,** Representative PCR product of PGC-1α and TIGAR from two patient-derived CAF lines treated with bFGF (100 ng/mL); β-actin served as loading control. **G,** Representative immunoblot of TFAM from two patient-derived CAF lines treated with bFGF (100 ng/mL). β-Actin served as loading control.

glucose conditions (26). Recently, FGFR was shown to activate mitochondrial pyruvate dehydrogenase kinase-1 (PDK1) and regulate the metabolic activity of cancer cells (27). Based upon this, we hypothesized HNSCC-secreted bFGF mediates and alters CAF metabolism. In support of this, we observed HNSCC-CM to increase CAF migration, invasion and proliferation in an FGFR-dependent manner (Fig. 4A–C). In order to determine whether mitochondrial OXPHOS was necessary for CAF proliferation, we treated CAFs with increasing doses of rotenone, a mitochondrial complex I inhibitor to determine the $IC_{50}$ value. We then used half the $IC_{50}$ to inhibit mitochondrial OXPHOS without inducing cell cytotoxicity over 72 hours. Our data demonstrate that rotenone treatment significantly attenuated bFGF induction of CAF proliferation ($P < 0.0001$; Fig. 4D). This indicates the regulation of OXPHOS in CAFs is necessary to obtain the proliferation phenotype. We assessed OXPHOS in CAFs treated with HNSCC-CM with or without pan-FGFR inhibitor, AZD-4547. HNSCC-CM increases maximal respiration in CAFs, which is mitigated by AZD-4547 [HN5-CM ($P < 0.0001$) and UM-SCC-1 ($P = 0.002$); Fig. 4E]. These results suggest HNSCC-secreted bFGF plays an important role in the regulation of OXPHOS in CAFs.

Expression of TIGAR promotes mitochondrial OXPHOS in breast carcinoma cells through the utilization of lactate and glutamate (28). In addition, TIGAR hydrolyses fructose-2,6-bisphosphate and fructose-1,6-bisphosphate decreasing their levels and consequently reducing glycolysis (15). We tested the effect of bFGF on TIGAR mRNA levels in two patient-derived CAF lines. Our data demonstrate that bFGF induced the expression of TIGAR in both CAF lines (Fig. 4F). In addition, FGF signaling has previously been associated with activation of peroxisome proliferator-activated receptor γ coactivator-1α (PGC-1α; ref. 29). PGC-1α is a well-known regulator of mitochondrial OXPHOS (30–32). In CAFs, bFGF induced PGC-1α expression (Fig. 4F). PGC-1α enhances the transcription of transcription factor A, mitochondrial (TFAM), an important transcription factor in mitochondrial biogenesis and OXPHOS (31, 32). bFGF induces the expression of TFAM in CAFs (Fig. 4G). These data indicate that bFGF attenuates CAF glycolysis through increased transcription of TIGAR and stimulates CAF OXPHOS by inducing the expression of PGC-1α and TFAM.

These results demonstrate HNSCC-secreted bFGF regulates CAF OXPHOS, proliferation, migration, and invasion. Moreover, FGFR inhibition did not return CAF proliferation and migration to baseline levels, indicating a role for other HNSCC-secreted factors. Nonetheless, these data support HNSCC-secreted bFGF as a key factor responsible for the induction of CAF mitochondrial OXPHOS, proliferation, and migration. This finding is particularly important as invasive CAFs may lead the metastatic cascade (33).

### HNSCC-secreted bFGF regulates HGF secretion from CAFs

Because HNSCC induces CAF HGF secretion (5), we assessed whether CAF-secreted HGF was a consequence of HNSCC-secreted bFGF. We demonstrate FGFR inhibition significantly reduces HNSCC-CM–induced HGF expression and secretion from CAFs [CAF-1 ($P = 0.021$), CAF-2 ($P = 0.029$), and CAF-3 ($P = 0.020$); Fig. 5A–C]. With this observation, we wanted to further delineate the mechanism of bFGF regulating HGF. Activation of FGFR triggers phosphorylation and signaling through p44/42 MAPK. We found HNSCC-CM significantly induced phosphorylation of p44/42 MAPK in CAFs, which was attenuated by FGFR inhibition ($P = 0.033$; Fig. 5D and E). Moreover, p44/42 MAPK inhibition with U0126 decreased HGF expression in CAFs (Fig. 5F). Taken together, these results suggest that HNSCC-secreted bFGF induces p44/42 MAPK phosphorylation, which in turn regulates HGF production in CAFs.

### Combined inhibition of c-Met and FGFR inhibits CAF-facilitated HNSCC proliferation *in vitro* and xenograft growth *in vivo*

With this reciprocal symbiosis, we sought to determine the effect of combinatorial c-Met and FGFR inhibition in HNSCC–CAF models. HNSCC rapidly proliferates in the presence of CAFs, with a 2-fold increase observed (Fig. 6A). Using combined treatment with c-Met inhibitor PF-02341066 and FGFR inhibitor AZD-4547, HNSCC proliferation induced by CAFs was significantly decreased compared with either single agent alone ($P < 0.0001$; Fig. 6A). In cocultured cells, the reciprocal activation of c-Met on HNSCC and FGFR on CAFs further induces signaling, resulting in increased tumor glycolysis and growth. Combined inhibition of both receptors in admixed cultures interferes with the reciprocal signaling between the two cell types. Thus, the combination treatment group reduced HNSCC proliferation below CAF-induced levels. We assessed the combinatorial effect by Bliss analysis and found the combination of PF-02341066 and AZD-4547 to be additive in nature (Supplementary Fig. S4A). The combined inhibition of both cell populations potentiates the effect of targeting cell population alone and demonstrates the therapeutic relevance of combination therapy *in vitro*.

We previously observed CAF and HNSCC xenograft tumors grow at a faster rate than HNSCC alone (5). Thus, we sought to determine the antitumor efficacy of combined inhibition of c-Met and FGFR in an admixed HNSCC-CAF model. HNSCC (UM-SCC-1) cells admixed with CAFs (2:1 ratio) were injected subcutaneously in the flank of athymic nude-Foxn1nu mice. Established tumor-bearing mice were treated orally every day with vehicle control, PF-02341066 (15 mg/kg every day), AZD-4547 (15 mg/kg every day), or the combination of PF-02341066 and AZD-4547 (15 mg each/kg every day) for 5 days a week. Combined treatment with PF-02341066 and AZD-4547 demonstrated significant reduction in tumor volume compared with treatment with either agent alone ($P < 0.001$; Fig. 6B). Moreover, the reduction in tumor weight on combined treatment was significantly decreased compared with either PF-02341066 ($P = 0.035$) or AZD-4547 ($P = 0.048$) treatment alone (Fig. 6C and D). No significant differences were observed in HNSCC-only xenografts (Supplementary Fig. S4B). Taken together, our data suggest that combined inhibition of FGFR and c-Met has greater antitumor effects than either agent alone.

## Discussion

In spite of recent advances in cancer treatment, current therapies for HNSCC are associated with poor survival and high morbidity. Innovative therapeutic strategies are needed for improved treatment of this disease. Despite a long-known recognition that the enhanced proliferation of cancer cells is associated with altered energy metabolism, no therapeutics are clinically available for patients with HNSCC that target metabolism. In

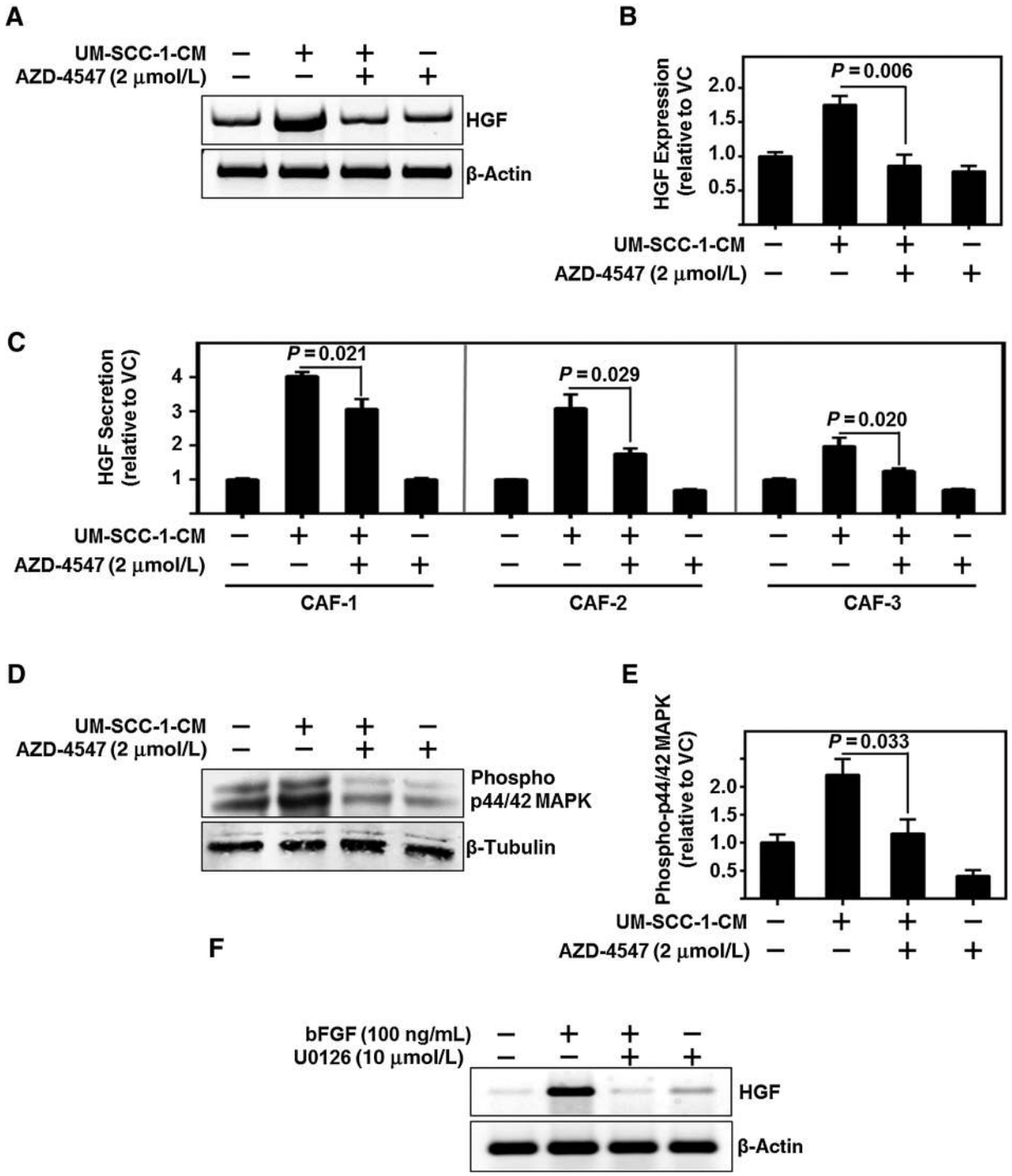


**Figure 5.**

HNSCC cells regulate HGF levels in CAFs via FGFR and MAPK. **A** and **B,** Representative PCR product of HGF and β-actin (used as loading control) in CAFs treated with UM-SCC-1-CM and/or FGFR inhibitor, AZD-4547 (2 μmol/L). Graph depicts cumulative results of three independent experiments. **C,** ELISA protein assessment of HGF secreted from three CAF lines treated with UM-SCC-1-CM and/or AZD4547 (2 μmol/L). Graph depicts cumulative results from three independent experiments normalized to vehicle control-treated CAF. **D** and **E,** Representative immunoblot of phospho–p44/42 MAPK and β-tubulin (used as loading control) in CAFs treated with UM-SCC-1-CM and/or AZD4547 (2 μmol/L). Graph depicts cumulative results from three independent experiments of phospho–p44/42 MAPK/β-tubulin normalized to vehicle control-treated CAFs. **F,** Representative PCR product of HGF and β-actin (used as loading control) of CAF treated with either bFGF (100 ng/mL) and/or p44/42 MAPK inhibitor, U0126 (10 μmol/L).

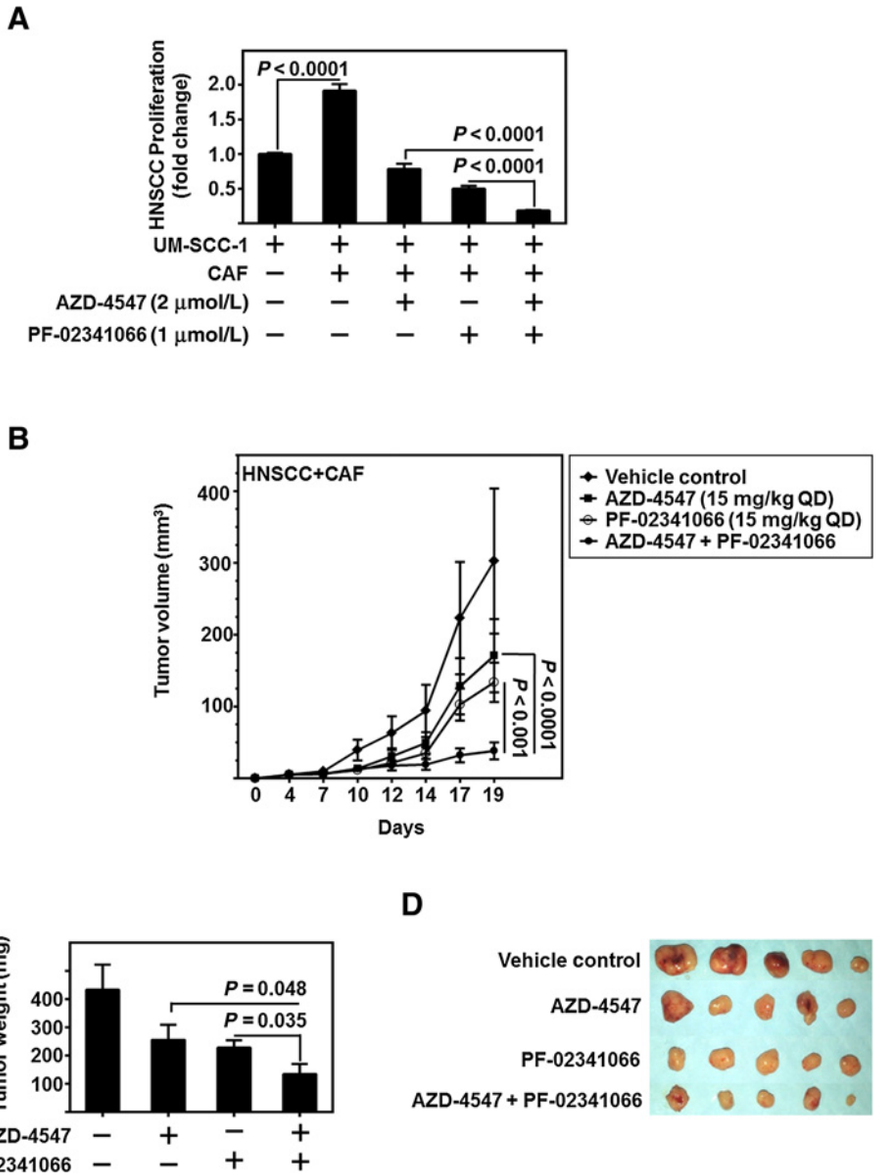


**Figure 6.**
Dual inhibition of c-Met and FGFR reduces HNSCC tumor growth *in vitro* and *in vivo*. **A,** CAF-facilitated UM-SCC-1 proliferation attenuated in FGFR inhibitor, AZD-4547 (2 μmol/L), or c-Met inhibitor, PF-02341066 (1 μmol/L), or combination of AZD-4547 and PF-02341066. Graph depicts cumulative results of CFSE-sorted UM-SCC-1 counted by flow cytometry from three independent experiments and normalized to UM-SCC-1 alone with no CAFs. **B,** CAF ($0.5 \times 10^6$ cells)-HNSCC ($1 \times 10^6$ cells) admixed tumor inoculated subcutaneously in athymic nude-Foxn1nu mice volume decreases with treatment of AZD-4547 [15 mg/kg every day (QD)] and/or PF-02341066 (15 mg/kg every day; $n = 5$/group). **C,** Graph depicts mean tumor weight of each treatment group from admixed CAF-HNSCC xenograft experiment depicted in **B**. Error bars, ± SEM. **D,** Gross images of tumors excised from CAF-HNSCC xenograft experiment depicted in **B**.

addition, the underlying biology explaining a mechanism for dysregulated metabolism is poorly understood. We find in this study that CAFs promote HNSCC glycolysis and act as a cellular compartment to sequester and use the resultant lactate. This creates a metabolic symbiosis where both cell types feed off each other to enhance proliferation, migration, and progression of this disease (Fig. 7).

A large portion of late-stage HNSCC tumors consists of CAFs. An increased ratio of CAFs to HNSCC correlates with increased tumor volume (34). In addition, migrating HNSCC-derived CAFs lead the invasive front in the metastatic process (33). Reciprocal signaling between the tumor and stroma has been reported in several cancers to facilitate tumor growth, invasion and resistance to therapy. Even though great strides have been made in understanding cancer cell metabolism, there exists a large gap in the knowledge pertaining to metabolic symbiosis between the tumor and cells in the microenvironment.

Previously, we reported that CAFs enhance HNSCC growth and metastasis (4, 5). Furthermore, we and others reported that c-Met and its ligand HGF are overexpressed in various cancer types including HNSCC (4, 35). Although we could not detect HGF secretion from HNSCC cell lines (Supplementary Fig. S2A), we reported that paracrine activation of c-Met by CAF-secreted HGF facilitates HNSCC progression (4). Very little is known about the regulation of HGF in CAFs and its impact on HNSCC metabolism.

HNSCC tumors are highly glycolytic and are routinely diagnosed using $^{18}$F-fluorodeoxyglucose PET ($^{18}$F-FDG-PET) imaging. $^{18}$F-FDG uptake in HNSCC tumors correlates with high lactate levels, poor prognosis, and reduced survival (36). In addition to glycolysis, glutaminolysis also produces lactate in cancer cells. However, it has been demonstrated that glucose, not glutamine, is the dominant energy source in a panel of 15 HNSCC cell lines (37).

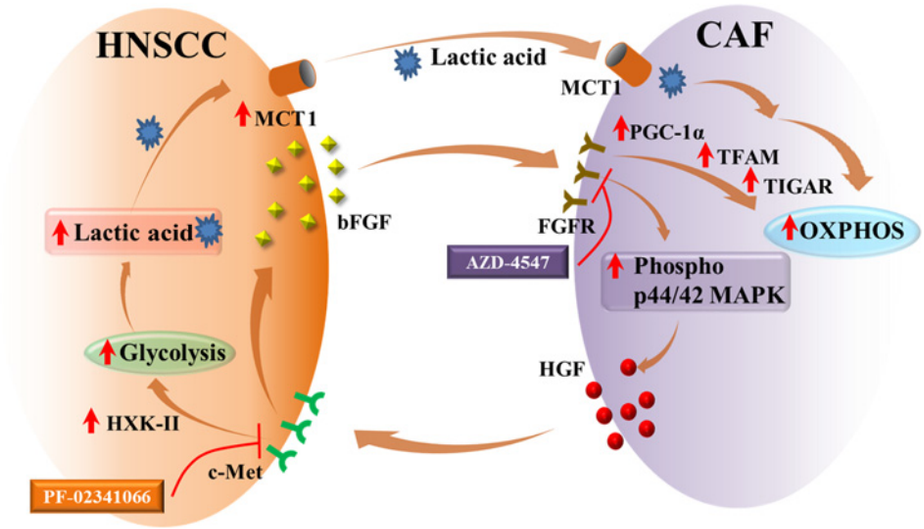


**Figure 7.**

Schematic representation of tumor–stroma metabolic symbiosis. HNSCC-secreted bFGF increases p44/42 MAPK phosphorylation, which induces secretion of HGF from CAFs, which bind to the c-Met receptor on HNSCC cells inducing secretion of bFGF from HNSCC cells. Furthermore, HGF regulates the expression of hexokinase-II (HXK-II) and increases cellular glycolysis. Lactic acid produced through glycolysis is transported out of the cells by monocarboxyl transporter 1 (MCT1). The lactic acid is used by CAFs as a source of energy through OXPHOS. OXPHOS in CAFs is induced by agonization of FGFR by bFGF. This induces increased expression of PGC-1α and TFAM, which increase OXPHOS. In addition, bFGF induces the expression of TIGAR (p53-inducible regulator of glycolysis and apoptosis), which downregulates glycolysis and increases OXPHOS. All in all, CAFs and HNSCC metabolically couple to facilitate tumor progression, and targeting this symbiosis inhibits tumor growth.

Lactate produced as a byproduct of glycolysis is actively transported out of the cell by MCT1, a bidirectional lactate transporter that is overexpressed in several tumors (38). MCT1 inhibition decreases lactate efflux, proliferation, cell biomass, migration, and invasion in breast cancer cells (39). A high level of stromal MCT1 is a negative prognostic factor in non–small cell lung cancer (40). Our data demonstrate an increase in MCT1 levels in admixed cultures of HNSCC and CAFs. C-Met inhibition reduced MCT1 levels and lactate production in HNSCC cells. This corroborates reports that link MET signaling intermediates MAPK and STAT3 with MCT1 (41, 42).

Expression of FGFR and its ligands has been reported in various cancers, including HNSCC (43). FGFR plays a pivotal role in tumorigenesis by regulating a multitude of processes, including cell survival, proliferation, metastasis, and angiogenesis (44). FGFR has been linked to metabolic alterations as FGFR knockout mice demonstrate altered metabolism, and FGFR1 directly regulates mitochondrial respiration through indication of PGC-1α (45, 46). Our data demonstrate that bFGF stimulation of CAFs induces the expression of PGC-1α and its downstream target TFAM. TFAM is a stimulatory component of the transcriptional complex that regulates the expression of all 13 proteins encoded by mitochondrial DNA that function as essential subunits of respiratory complexes I, III, IV, and V (47). In addition, we demonstrate increased transcription of TIGAR in CAFs. TIGAR hydrolyses fructose-2,6-bisphosphate and fructose-1,6-bisphosphate, decreasing their levels and consequently reducing glycolysis in nasopharyngeal carcinoma (15). In addition, TIGAR promotes mitochondrial OXPHOS in breast carcinoma cells through the utilization of lactate and glutamate (28). Increased expression of TIGAR, PGC-1α, and TFAM on bFGF stimulation in CAFs indicates the mechanism by which CAFs undergo metabolic reprogramming to enhance OXPHOS.

In this work, we demonstrate that c-Met inactivation alters HNSCC metabolism alongside a mitigation of CAF-stimulated bFGF protein secretion from HNSCC. Activation of multiple signaling pathways occurs downstream of HGF/c-Met. These include p44/42 MAPK (p44/42 MAPK) and PI3K/Akt (48). Furthermore, FGFR inhibition reduced both HNSCC and stromal compartments in xenograft models (8). Our data corroborate and extend previous reports demonstrating bFGF-mediated FGFR activation triggers downstream p44/42 MAPK signaling, a well-known regulator of cell proliferation (49). Indeed, FGFR mediates proliferation of CAFs on stimulation with HNSCC conditioned media. Inhibition of mitochondrial OXPHOS using half the $IC_{50}$ dose of rotenone attenuated bFGF-induced CAF proliferation without significant cytotoxicity. Mitochondrial OXPHOS has been reported to be important for proliferation in other cell types (50, 51). In addition to regulating cell proliferation, our data demonstrate that HNSCC cells regulate HGF secretion from CAFs via FGFR. This finding is in agreement with previous reports demonstrating regulation of HGF secretion by bFGF in mesenchymal cells (52), and in murine cells (53). Together, these findings support our hypothesis of a dynamic reciprocal interaction between HNSCC and CAFs that facilitates HNSCC tumor metabolism and progression through c-Met/FGFR signaling as shown in Fig. 7.

Clinically relevant small-molecule c-Met inhibitor PF-02341066 (crizotinib) effectively reduces HNSCC growth *in vitro* and *in vivo* and circumvents acquired resistance to molecular targeted therapy (54). PF-02341066 is a competitive ATP inhibitor that induces apoptosis and inhibits cell proliferation, angiogenesis, migration, and invasion in multiple preclinical cancer

models. Furthermore, PF-02341066 potentiates the effects of radiation and chemotherapeutic agents. Here, we have shown that c-Met inhibition with PF-02341066 reduced glycolysis and bFGF expression in HNSCC. AZD-4547 is a clinically relevant small-molecule pyrazoloamide derivative, pan-FGFR tyrosine kinase inhibitor (55). AZD-4547 has been reported to inhibit progression of numerous cancers, and we demonstrate that FGFR inhibition with AZD-4547 reduces OXPHOS, proliferation, migration, and HGF expression in CAFs.

Based on our mechanistic insights, we tested the antitumor efficacy of FGFR inhibitor AZD-4547 in combination with c-Met inhibitor PF-02341066 both *in vitro* and *in vivo* and show, for the first time, that the combination treatment significantly inhibited HNSCC growth *in vitro* and *in vivo*. Our cumulative findings underscore the therapeutic potential of combinatorial treatment with PF-02341066 and AZD-4547 in HNSCC.

## Disclosure of Potential Conflicts of Interest

No potential conflicts of interest were disclosed.

## Authors' Contributions

**Conception and design:** J. New, O. Tawfik, Y. Shnayder, T.T. Tsue, S. Anant, S.M. Thomas

**Development of methodology:** D. Kumar, J. New, R. Joshi, W.R. Gutierrez, O. Tawfik, S.M. Thomas

**Acquisition of data (provided animals, acquired and managed patients, provided facilities, etc.):** D. Kumar, J. New, V. Vishwakarma, R. Joshi, J. Enders, F. Lin, S. Dasari, W.R. Gutierrez, G. Leef, H. Chavan, L. Ganaden, M.M. Thornton, O. Tawfik, J. Straub, K. Kakarala, B. Van Houten, P. Krishnamurthy, S.M. Thomas

**Analysis and interpretation of data (e.g., statistical analysis, biostatistics, computational analysis):** D. Kumar, J. New, V. Vishwakarma, R. Joshi, J. Enders, H. Dai, O. Tawfik, J. Straub, B. Van Houten, P. Krishnamurthy, S.M. Thomas

**Writing, review, and/or revision of the manuscript:** D. Kumar, J. New, J. Enders, F. Lin, L. Ganaden, H. Dai, O. Tawfik, J. Straub, Y. Shnayder, K. Kakarala, T.T. Tsue, D.A. Girod, B. Van Houten, S. Anant, P. Krishnamurthy, S.M. Thomas

**Administrative, technical, or material support (i.e., reporting or organizing data, constructing databases):** J. New, R. Joshi, S. Ponnurangam, D.A. Girod, S.M. Thomas

**Study supervision:** R. Joshi, Y. Shnayder, T.T. Tsue, S.M. Thomas

**Other (manuscript review):** V. Vishwakarma

**Other (provided expertise with Seahorse mitochondrial bioenergetics experimentation):** H. Chavan

## Acknowledgments

American Head and Neck Society Pilot Award (to S.M. Thomas), University of Kansas Medical Center and University of Kansas Cancer Center's CCSG (1-P30-CA168524-02; to S.M. Thomas), Postdoctoral Fellowship from the Institutional Development Award (IDeA), National Institute of General Medical Sciences, NIH (P20 GM103418; to D. Kumar), The KUMC Biomedical Research Training Program Fellowship (to J. New), 5P20RR021940-07 and 8P20GM103549-07 (to P. Krishnamurthy), CA190291 (to S. Anant), PA CURE award, and in part P30CA047904 (to B. Van Houten) were the funding sources. We acknowledge support from the University of Kansas Cancer Center, Biospecimen Repository Core Facility.

The costs of publication of this article were defrayed in part by the payment of page charges. This article must therefore be hereby marked *advertisement* in accordance with 18 U.S.C. Section 1734 solely to indicate this fact.

Received April 20, 2017; revised December 13, 2017; accepted May 11, 2018; published first May 16, 2018.

## References

1. Matta A, Ralhan R. Overview of current and future biologically based targeted therapies in head and neck squamous cell carcinoma. Head Neck Oncol 2009;1:6.
2. Kim L, King T, Agulnik M. Head and neck cancer: changing epidemiology and public health implications. Oncology 2010;24:915–9.
3. Curry JM, Sprandio J, Cognetti D, Luginbuhl A, Bar-ad V, Pribitkin E, et al. Tumor microenvironment in head and neck squamous cell carcinoma. Semin Oncol 2014;41:217–34.
4. Knowles LM, Stabile LP, Egloff AM, Rothstein ME, Thomas SM, Gubish CT, et al. HGF and c-Met participate in paracrine tumorigenic pathways in head and neck squamous cell cancer. Clin Cancer Res 2009;15:3740–50.
5. Wheeler S, Shi H, Lin F, Dasari S, Bednash J, Thorne S, et al. Enhancement of head and neck squamous cell carcinoma proliferation, invasion, and metastasis by tumor-associated fibroblasts in preclinical models. Head Neck 2014;36:385–92.
6. Riedel F, Gotte K, Bergler W, Rojas W, Hormann K. Expression of basic fibroblast growth factor protein and its down-regulation by interferons in head and neck cancer. Head Neck 2000;22:183–9.
7. Vairaktaris E, Ragos V, Yapijakis C, Derka S, Vassiliou S, Nkenke E, et al. FGFR-2 and -3 play an important role in initial stages of oral oncogenesis. Anticancer Res 2006;26:4217–21.
8. Sweeny L, Liu Z, Lancaster W, Hart J, Hartman YE, Rosenthal EL. Inhibition of fibroblasts reduced head and neck cancer growth by targeting fibroblast growth factor receptor. Laryngoscope 2012;122:1539–44.
9. Pedersen PL. Warburg, me and hexokinase 2: Multiple discoveries of key molecular events underlying one of cancers' most common phenotypes, the "Warburg Effect", i.e., elevated glycolysis in the presence of oxygen. J Bioenerg Biomembr 2007;39:211–22.
10. Gray LR, Tompkins SC, Taylor EB. Regulation of pyruvate metabolism and human disease. Cell Mol Life Sci 2014;71:2577–604.
11. Curry JM, Tuluc M, Whitaker-Menezes D, Ames JA, Anantharaman A, Butera A, et al. Cancer metabolism, stemness and tumor recurrence: MCT1 and MCT4 are functional biomarkers of metabolic symbiosis in head and neck cancer. Cell Cycle 2013;12:1371–84.
12. Sano D, Xie T-X, Ow TJ, Zhao M, Pickering CR, Zhou G, et al. Disruptive TP53 mutation is associated with aggressive disease characteristics in an orthotopic murine model of oral tongue cancer. Clin Cancer Res 2011;17:6658–70.
13. Keeton EK, Brown M. Cell cycle progression stimulated by tamoxifen-bound estrogen receptor-α and promoter-specific effects in breast cancer cells deficient in N-CoR and SMRT. Mol Endocrinol 2005;19:1543–54.
14. Wheeler SE, Shi H, Lin F, Dasari S, Bednash J, Thorne S, et al. Tumor associated fibroblasts enhance head and neck squamous cell carcinoma proliferation, invasion, and metastasis in preclinical models. Head Neck 2014;36:385–92.
15. Lui VW, Wong EY, Ho K, Ng PK, Lau CP, Tsui SK, et al. Inhibition of c-Met downregulates TIGAR expression and reduces NADPH production leading to cell death. Oncogene 2011;30:1127–34.
16. Jiang P, Du W, Mancuso A, Wellen KE, Yang X. Reciprocal regulation of p53 and malic enzymes modulates metabolism and senescence. Nature 2013;493:689–93.
17. Li B, Qiu B, Lee DS, Walton ZE, Ochocki JD, Mathew LK, et al. Fructose-1,6-bisphosphatase opposes renal carcinoma progression. Nature 2014;513:251–5.
18. Varkaris A, Gaur S, Parikh NU, Song JH, Dayyani F, Jin J-K, et al. Ligand-independent activation of MET through IGF-1/IGF-1R signaling. Int J Cancer 2013;133:1536–46.
19. Li L, Puliyappadamba VT, Chakraborty S, Rehman A, Vemireddy V, Saha D, et al. EGFR wild type antagonizes EGFRvIII-mediated activation of Met in glioblastoma. Oncogene 2015;34:129–34.
20. Mathupala SP, Ko YH, Pedersen PL. Hexokinase II: Cancer's double-edged sword acting as both facilitator and gatekeeper of malignancy when bound to mitochondria. Oncogene 2006;25:4777–86.
21. Kennedy KM, Dewhirst MW. Tumor metabolism of lactate: the influence and therapeutic potential for MCT and CD147 regulation. Future Oncol 2010;6:127–48.

22. Hughes SE. Differential expression of the fibroblast growth factor receptor (FGFR) multigene family in normal human adult tissues. J Histochem Cytochem 1997;45:1005–19.
23. Dellacono FR, Spiro J, Eisma R, Kreutzer D. Expression of basic fibroblast growth factor and its receptors by head and neck squamous carcinoma tumor and vascular endothelial cells. Am J Surg 1997;174: 540–4.
24. Mansukhani A, Bellosta P, Sahni M, Basilico C. Signaling by fibroblast growth factors (FGF) and fibroblast growth factor receptor 2 (FGFR2)-activating mutations blocks mineralization and induces apoptosis in osteoblasts. J Cell Biol 2000;149:1297–308.
25. Zhang D, Wang Y, Shi Z, Liu J, Sun P, Hou X, et al. Metabolic reprogramming of cancer-associated fibroblasts by IDH3alpha downregulation. Cell Rep 2015;10:1335–48.
26. Chaudhri VK, Salzler GG, Dick SA, Buckman MS, Sordella R, Karoly ED, et al. Metabolic alterations in lung cancer-associated fibroblasts correlated with increased glycolytic metabolism of the tumor. Mol Cancer Res 2013;11:579–92.
27. Hitosugi T, Fan J, Chung TW, Lythgoe K, Wang X, Xie JX, et al. Tyrosine phosphorylation of mitochondrial pyruvate dehydrogenase kinase 1 is important for cancer metabolism. Mol Cell 2011;44: 864–77.
28. Ko Y-H, Domingo-Vidal M, Roche M, Lin Z, Whitaker-Menezes D, Seifert E, et al. TIGAR metabolically reprograms carcinoma and stromal cells in breast cancer. J Biol Chem 2016;291:26291–303.
29. Potthoff MJ, Inagaki T, Satapati S, Ding X, He T, Goetz R, et al. FGF21 induces PGC-1alpha and regulates carbohydrate and fatty acid metabolism during the adaptive starvation response. Proc Natl Acad Sci U S A 2009; 106:10853–8.
30. LeBleu VS, O'Connell JT, Gonzalez Herrera KN, Wikman H, Pantel K, Haigis Marcia C, et al. PGC-1α mediates mitochondrial biogenesis and oxidative phosphorylation in cancer cells to promote metastasis. Nat Cell Biol 2014;16:992.
31. Deblois G, St-Pierre J, Giguere V. The PGC-1/ERR signaling axis in cancer. Oncogene 2013;32:3483–90.
32. Lin J, Handschin C, Spiegelman BM. Metabolic control through the PGC-1 family of transcription coactivators. Cell Metab 2005;1:361–70.
33. Gaggioli C, Hooper S, Hidalgo-Carcedo C, Grosse R, Marshall JF, Harrington K, et al. Fibroblast-led collective invasion of carcinoma cells with differing roles for RhoGTPases in leading and following cells. Nat Cell Biol 2007;9:1392–400.
34. Bae JY, Kim EK, Yang DH, Zhang X, Park YJ, Lee DY, et al. Reciprocal interaction between carcinoma-associated fibroblasts and squamous carcinoma cells through interleukin-1alpha induces cancer progression. Neoplasia 2014;16:928–38.
35. Di Renzo MF, Poulsom R, Olivero M, Comoglio PM, Lemoine NR. Expression of the Met/hepatocyte growth factor receptor in human pancreatic cancer. Cancer Res 1995;55:1129–38.
36. Yamada T, Uchida M, Kwang-Lee K, Kitamura N, Yoshimura T, Sasabe E, et al. Correlation of metabolism/hypoxia markers and fluorodeoxyglucose uptake in oral squamous cell carcinomas. Oral Surg Oral Med Oral Pathol Oral Radiol 2012;113:464–71.
37. Sandulache VC, Ow TJ, Pickering CR, Frederick MJ, Zhou G, Fokt I, et al. Glucose, not glutamine, is the dominant energy source required for proliferation and survival of head and neck squamous carcinoma cells. Cancer 2011;117:2926–38.
38. Doherty JR, Cleveland JL. Targeting lactate metabolism for cancer therapeutics. J Clin Invest 2013;123:3685–92.
39. Morais-Santos F, Granja S, Miranda-Goncalves V, Moreira AH, Queiros S, Vilaca JL, et al. Targeting lactate transport suppresses in vivo breast tumour growth. Oncotarget 2015;6:19177–89.
40. Koukourakis MI, Giatromanolaki A, Bougioukas G, Sivridis E. Lung cancer: a comparative study of metabolism related protein expression in cancer cells and tumor associated stroma. Cancer Biol Ther 2007;6:1476–9.
41. Bhalla S, Evens AM, Dai B, Prachand S, Gordon LI, Gartenhaus RB. The novel anti-MEK small molecule AZD6244 induces BIM-dependent and AKT-independent apoptosis in diffuse large B-cell lymphoma. Blood 2011;118:1052–61.
42. Silva LS, Goncalves LG, Silva F, Domingues G, Maximo V, Ferreira J, et al. STAT3:FOXM1 and MCT1 drive uterine cervix carcinoma fitness to a lactate-rich microenvironment. Tumor Biol 2016;37:5385–95.
43. Marshall ME, Hinz TK, Kono SA, Singleton KR, Bichon B, Ware KE, et al. Fibroblast growth factor receptors are components of autocrine signaling networks in head and neck squamous cell carcinoma cells. Clin Cancer Res 2011;17:5016–25.
44. Katoh M, Nakagama H. FGF receptors: cancer biology and therapeutics. Med Res Rev 2014;34:280–300.
45. Ornitz DM, Itoh N. The fibroblast growth factor signaling pathway. Wiley Interdiscip Rev Dev Biol 2015;4:215–66.
46. Mäkelä J, Tselykh TV, Maiorana F, Eriksson O, Do HT, Mudò G, et al. Fibroblast growth factor-21 enhances mitochondrial functions and increases the activity of PGC-1α in human dopaminergic neurons via Sirtuin-1. SpringerPlus 2014;3:2.
47. Scarpulla RC. Nuclear control of respiratory chain expression by nuclear respiratory factors and PGC1related coactivator. Ann N Y Acad Sci 2008;1147:321–34.
48. Usatyuk PV, Fu PF, Mohan V, Epshtein Y, Jacobson JR, Gomez-Cambronero J, et al. Role of c-Met/phosphatidylinositol 3-kinase (PI3k)/Akt signaling in hepatocyte growth factor (HGF)- mediated lamellipodia formation, reactive oxygen species (ROS) generation, and motility of lung endothelial cells. J Biol Chem 2014;289:13476–91.
49. Yang H, Xia Y, Lu SQ, Soong TW, Feng ZW. Basic fibroblast growth factor-induced neuronal differentiation of mouse bone marrow stromal cells requires FGFR-1, MAPK/ERK, and transcription factor AP-1. J Biol Chem 2008;283:5287–95.
50. Weinberg F, Hamanaka R, Wheaton WW, Weinberg S, Joseph J, Lopez M, et al. Mitochondrial metabolism and ROS generation are essential for Kras-mediated tumorigenicity. Proc Natl Acad Sci 2010;107:8788–93.
51. Birsoy K, Wang T, Chen Walter W, Freinkman E, Abu-Remaileh M, Sabatini David M. An essential role of the mitochondrial electron transport chain in cell proliferation is to enable aspartate synthesis. Cell 2015;162:540–51.
52. Roletto F, Galvani AP, Cristiani C, Valsasina B, Landonio A, Bertolero F. Basic fibroblast growth factor stimulates hepatocyte growth factor/scatter factor secretion by human mesenchymal cells. J Cell Physiol 1996;166:105–11.
53. Onimaru M, Yonemitsu Y, Tanii M, Nakagawa K, Masaki I, Okano S, et al. Fibroblast growth factor-2 gene transfer can stimulate hepatocyte growth factor expression irrespective of hypoxia-mediated downregulation in ischemic limbs. Circ Res 2002;91:923–30.
54. Stabile LP, He G, Lui VW, Thomas S, Henry C, Gubish CT, et al. c-Src activation mediates erlotinib resistance in head and neck cancer by stimulating c-Met. Clin Cancer Res 2013;19:380–92.
55. Gavine PR, Mooney L, Kilgour E, Thomas AP, Al-Kadhimi K, Beck S, et al. AZD4547: an orally bioavailable, potent, and selective inhibitor of the fibroblast growth factor receptor tyrosine kinase family. Cancer Res 2012;72:2045–56.